

First direct measurement of the $^{23}\text{Mg}(p,\gamma)^{24}\text{Al}$ reaction

L. Erikson,¹ C. Ruiz,^{2,*} F. Ames,² P. Bricault,² L. Buchmann,² A. A. Chen,³ J. Chen,³ H. Dare,⁴ B. Davids,² C. Davis,² C. M. Deibel,^{5,6} M. Dombisky,² S. Foubister,⁷ N. Galinski,² U. Greife,¹ U. Hager,² A. Hussein,⁸ D. A. Hutcheon,² J. Lassen,² L. Martin,² D. F. Ottewell,² C. V. Ouellet,³ G. Ruprecht,² K. Setoodehnia,³ A. C. Shotter,⁹ A. Teigelhöfer,² C. Vockenhuber,^{2,10} C. Wrede,¹¹ and A. Wallner¹²

¹*Department of Physics, Colorado School of Mines, Golden, Colorado 80401, USA*

²*TRIUMF, Vancouver, British Columbia V6T 2A3, Canada*

³*McMaster University, Hamilton, Ontario L8S 481, Canada*

⁴*University of Surrey, Guildford, GU2 7XH, England, United Kingdom*

⁵*Physics Division, Argonne National Laboratory, Illinois 60439, USA*

⁶*Joint Institute for Nuclear Astrophysics, Michigan State University, East Lansing, Michigan 48824, USA*

⁷*Thompson Rivers University, Kamloops, British Columbia V2C 5N3, Canada*

⁸*University of Northern British Columbia, Prince George, British Columbia V2N 4Z9, Canada*

⁹*University of Edinburgh, Edinburgh EH9 3JZ, Scotland, United Kingdom*

¹⁰*Laboratory of Ion Beam Physics, ETH Zurich, CH-8093 Zurich, Switzerland*

¹¹*University of Washington, Seattle, Washington 98195, USA*

¹²*University of Vienna, A-1010 Vienna, Austria*

(Received 17 September 2009; revised manuscript received 22 February 2010; published 29 April 2010)

The lowest-energy resonance in the $^{23}\text{Mg}(p,\gamma)^{24}\text{Al}$ reaction, which is dominant at classical nova temperatures, has been measured directly for the first time using the DRAGON recoil spectrometer. The experiment used a radioactive ^{23}Mg beam (mixed within a significantly stronger ^{23}Na beam) of peak intensity $5 \times 10^7 \text{ s}^{-1}$, at the ISAC facility at TRIUMF. We extract values of $E_R = 485.7_{-1.8}^{+1.3} \text{ keV}$ and $\omega\gamma = 38_{-15}^{+21} \text{ meV}$ from our data (all values in the center-of-mass frame unless otherwise stated). In addition, the experiment prompted a recalculation of the Q value for this reaction based on a revision of the ^{24}Al mass. The effect on the uncertainties in the quantities of ejected ^{22}Na and ^{26}Al from oxygen-neon classical novae is discussed.

DOI: [10.1103/PhysRevC.81.045808](https://doi.org/10.1103/PhysRevC.81.045808)

PACS number(s): 24.30.-v, 25.40.Lw, 26.50.+x, 27.30.+t

I. INTRODUCTION

The $^{23}\text{Mg}(p,\gamma)^{24}\text{Al}$ reaction is an important link between the Ne-Na and Mg-Al cycles in O-Ne classical novae. It provides an additional route for proton capture out of the Ne-Na cycle by bypassing the decay of ^{23}Mg ($t_{1/2} = 11.32 \text{ s}$), which forms stable ^{23}Na . At nova temperatures in the Ne-Na cycle, the $^{23}\text{Na}(p,\alpha)^{20}\text{Ne}$ reaction continues the cyclic flow, but around 50% of the time [1] the $^{23}\text{Na}(p,\gamma)^{24}\text{Mg}$ reaction provides a route out of the cycle. The $^{23}\text{Mg}(p,\gamma)^{24}\text{Al}$ reaction forms $^{24g,m}\text{Al}$ ($t_{1/2} = 2.07 \text{ s}$, 129 ms) which decays to ^{24}Mg and reaches the entrance to the Mg-Al cycle on a shorter time scale (see Fig. 1). Consequently, the strength of the $^{23}\text{Mg}(p,\gamma)^{24}\text{Al}$ reaction has a bearing on the synthesized amounts of radioactive ^{22}Na ($t_{1/2} = 2.604 \text{ y}$) and ^{26g}Al ($t_{1/2} = 7.1 \times 10^5 \text{ y}$) which are important targets of γ -ray astronomy.

In the reaction rate sensitivity study of Iliadis *et al.* [2], the uncertainty in the $^{23}\text{Mg}(p,\gamma)^{24}\text{Al}$ rate is given as a factor of 100 up and 100 down over the whole nova temperature range. This leads to a large uncertainty in the predicted ejected abundances of ^{22}Na and ^{26g}Al (e.g., model S1 of Ref. [2], with $T_{\text{peak}} = 0.418 \text{ GK}$) up to factors of 30 and 3 respectively. Of all the reactions in the mass region shown in Fig. 1 that are important at nova temperatures between 0.1 and 0.4 GK, $^{23}\text{Mg}(p,\gamma)^{24}\text{Al}$ and $^{25}\text{Al}(p,\gamma)^{26}\text{Si}$ are the only

ones that have remained unmeasured. This is primarily due to the difficulty of producing short-lived, accelerated radioactive ion beams of sufficient intensity and purity to make direct reaction rate measurements. In this work we describe the first such measurement of the $^{23}\text{Mg}(p,\gamma)^{24}\text{Al}$ reaction rate, performed in inverse kinematics at the DRAGON facility. This experiment used a high-intensity ^{23}Mg beam produced by the ISOL method at TRIUMF-ISAC in Vancouver, British Columbia, Canada.

II. PREVIOUS EXPERIMENTAL AND THEORETICAL WORK

A. Level and resonance energies, strengths, and assignments

There are several predicted resonances of astrophysical interest in the $^{23}\text{Mg}(p,\gamma)^{24}\text{Al}$ reaction. None of these have been studied directly, but the corresponding excited states have been investigated via particle and γ -ray spectroscopy. These experiments identified the first few levels above the proton separation energy in ^{24}Al which correspond to resonance energies of 473, 651, 739, and 920 keV in the center-of-mass system [3]. The lowest lying of these resonances is thought to be the dominant contributor to the $^{23}\text{Mg}(p,\gamma)^{24}\text{Al}$ reaction rate at nova temperatures [4] and is the focus of this work.

The most recent experimental value of the “473 keV” resonance energy comes from a fusion-evaporation study using the gammasphere array (Lotay *et al.* [5]). Its value of

* ruiz@triumf.ca

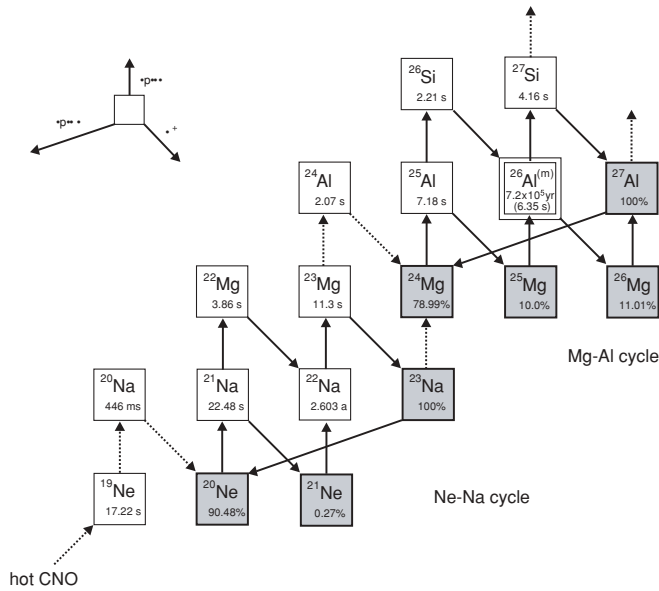


FIG. 1. The transition between the Ne-Na and Mg-Al cycles, showing typical contributing reactions at nova temperatures.

$E_R = 473 \pm 3$ keV is derived from a precise measurement of γ -ray energies to determine the excitation energy, followed by a subtraction of the proton separation energy of ^{24}Al . Provided that the identification of the populated state is correct, this should be the most precise experimental value of excitation energy because of the capability of γ -ray measurements. However, the other determinations of level energy from particle spectroscopy [3,6–8] show some spread. For example, the experiment of Kubono *et al.* [7] resulted in a value of $E_R = 456 \pm 10$ keV while the measurement of Greenfield *et al.* [6] gave a value of 497 ± 5 keV. The two most recent particle spectroscopy measurements with values of 474 ± 6 keV [3] and 477 ± 10 keV [8] are in good agreement with the measured level energy in the gammasphere experiment. All of these values of resonance energy are derived using either a Q value based on the masses of ^{23}Mg , p , and ^{24}Al as given in the Audi, Wapstra, and Thibault compilation [9] ($Q = 1872 \pm 3$ keV) or a method that is dependent on other nuclear masses. Table I presents the results of all previous measurements determining the energy of the astrophysically relevant state in ^{24}Al .

TABLE I. Summary of previous measurements of the energy of the first excited state above the proton threshold in ^{24}Al . Resonance energies are calculated using the Audi-Wapstra-Thibault [9] Q value of 1872 ± 3 keV. Also shown are adjusted resonance energies for the experiments of Refs. [3,5], based on a modern reevaluation of the ^{24}Al and ^{28}P mass excesses (for explanation, see Sec. II B).

Experiment	E_x (keV)	E_R (keV)	E_R^{adjusted} (keV)
$^{24}\text{Mg}(^3\text{He},t)^{24}\text{Al}$ [6]	2369(4)	497(5)	–
$^{24}\text{Mg}(^3\text{He},t)^{24}\text{Al}$ [7]	2328(10)	456(10)	–
$^{24}\text{Mg}(^3\text{He},t)^{24}\text{Al}$ [3]	2346(6)	474(6)	480(6)
$^{24}\text{Mg}(^3\text{He},t)^{24}\text{Al}$ [8]	2349(10)	477(10)	–
$^{10}\text{B}(^{16}\text{O},2n\gamma)^{24}\text{Al}$ [5]	2345.1(14)	473(3)	482.5(33)

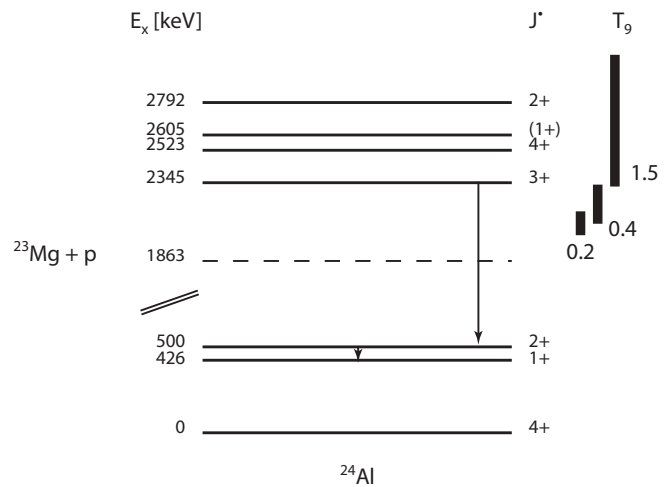


FIG. 2. Level diagram of states in ^{24}Al above the proton threshold. The Gamow windows for different temperatures (in GK) are shown at the right.

The ^{24}Al level scheme in Ref. [5] gives the energy of the first level above proton threshold as 2345.1(14) keV with a tentative spin-parity assignment of $J^\pi = (3^+)$. The spin and parity assignment is based on shell-model calculations [4] and has not been verified experimentally (Fig. 2).

An initial experiment at DRAGON to measure the “473 keV” resonance was performed in inverse kinematics using a ^{23}Mg beam energy of 497.8A keV. This energy was chosen to cover the center-of-mass energy range $E_{\text{c.m.}} = 453.2\text{--}480.5$ keV, which would fully contain the Lotay *et al.* [5] resonance energy and the upper half of the range of the Kubono *et al.* [7] uncertainty, within the DRAGON hydrogen gas target operating at 10.5 mbar. However, during this experiment an ISOL target failure resulted in insufficient beam to satisfactorily measure a resonance strength, and no ^{24}Al recoils were detected. Therefore only upper limits were set on the resonance strength of $\omega\gamma \leq 3.6$ meV in the energy range $E_{\text{c.m.}} = 458.3\text{--}480.5$ keV and $\omega\gamma \leq 18.4$ meV in the range $E_{\text{c.m.}} = 453.2\text{--}458.3$ keV (see Ref. [10] for details). Both of these values are significantly below the predicted shell-model strength of 27 meV [4].

B. The reaction Q value

After completion of the analysis of the first ^{23}Mg experiment, the failure to detect the expected resonance motivated a closer look at all the input parameters used to determine the beam energy and range of possible resonance energies. In an investigation of mass measurements reported in literature subsequent to the work described in Secs. III and IV, it was found that the ^{24}Al proton-separation energy reported in the Audi, Wapstra, and Thibault Atomic Mass Evaluation (AME03) [9] might be misleading. It is based on a 1976 recalibration [11] of a prior $^{24}\text{Mg}(p,n)^{24}\text{Al}$ threshold measurement by Overley *et al.* [12]. In Ref. [12] the $^{24}\text{Mg}(p,n)^{24}\text{Al}$ threshold was determined with reference to a number of known (p,n)

thresholds that were used to calibrate the magnet constant of an analyzing magnet that selected the beam energy.

We reevaluated the threshold energies for these calibration reactions using the AME03 masses as inputs in every case except for $^{54}\text{Fe}(p,n)^{54}\text{Co}$. There the effective threshold of 9204.3(20) keV was adopted based on the Q_{EC} value of Ref. [13]. The difference between the true threshold and the effective threshold was estimated to be 8(2) keV from Fig. 1 of Ref. [14]. Using this value yielded a new magnet constant of 44.239(7) for the experiments described by Overley *et al.* [12]. Applying this magnet constant to the $^{24}\text{Mg}(p,n)^{24}\text{Al}$ measurement yields a new value of 15289.3 keV for the threshold energy, corresponding to a Q value of $-14668.5(26)$ keV. In turn, this yields a new mass excess $\Delta(^{24}\text{Al}) = -47.4(2.6)$ keV, which, together with the AME03 values for ^{23}Mg and ^1H , yields $Q(^{23}\text{Mg}(p,\gamma)^{24}\text{Al}) = 1862.6(2.9)$ keV. Combining this value with the excitation energy from Ref. [5] yields $E_R = 482.5(3.3)$ keV. This is 9.5 keV higher than the value obtained by taking the AME03 masses at face value combined with the γ energies of Ref. [5].

A somewhat similar treatment may be applied to the data of Visser *et al.* [3] where the resonance energy is independent of the ^{24}Al mass and depends instead on the ^{28}P mass via the calibration reaction. In AME03, the ^{28}P mass was derived in part from the $^{28}\text{Si}(p,n)^{28}\text{P}$ threshold measurements of Overley *et al.* [12] mentioned above, and from a subsequent measurement [15] of the same reaction that used the $^{24}\text{Mg}(p,n)^{24}\text{Al}$ threshold value from Ref. [12] as a primary calibration standard. Applying the new magnet constant above yields a new value of 15672.1 keV for the $^{28}\text{Si}(p,n)^{28}\text{P}$ threshold from Ref. [12], corresponding to a Q value of $-15123.1(39)$ keV. Adjusting the $^{28}\text{Si}(p,n)^{28}\text{P}$ threshold measurement in Ref. [15] by using our new $^{24}\text{Mg}(p,n)^{24}\text{Al}$ threshold yields a new value of 15669.0 keV, corresponding to a Q value of $-15120.2(60)$ keV. The weighted average of these two Q -value measurements is $-15122.3(33)$ keV, which yields a new mass excess $\Delta(^{28}\text{P}) = -7152.9(33)$ keV. This is 6.1 keV higher than the AME03 value. Thus, the resonance energy of $E_R = 474$ keV reported in Ref. [3] may be adjusted to a new value of $E_R = 473.5 + 6.1 = 480(6)$ keV.

The adjusted values for E_R are summarized alongside the previously reported values in Table I. The table shows that the resonance energy could be on the order of 10 keV higher than previously reported. Beam energies for the second ^{23}Mg experiment were chosen based on the previous null measurement of the $^{23}\text{Mg}(p,\gamma)$ reaction at the relatively lower energies mentioned in Sec. II A. It will be later seen in Sec. IV D that the adjusted resonance energies agree with our direct determination.

III. EXPERIMENTAL PROCEDURE

The ^{23}Mg beam was created at the ISAC facility by bombarding a series of silicon-carbide/graphite composite foils with a 500-MeV proton beam at $35 \mu\text{A}$, reaching an effective target temperature of 1700°C . TRIUMF's Resonant Ionization Laser Ion Source (TRILIS) was used in order to selectively boost the ionization efficiency for magnesium [16],

and ions were extracted from the target/ion-source assembly using a potential difference of 46.9 kV.

$A = 23$ products were selected using a high-resolution mass separator and accelerated to the beam energies of interest using the ISAC accelerators, consisting of a radiofrequency quadrupole (RFQ) device providing fixed acceleration to 150A keV and then a continuously variable energy (150A keV–1850A keV) drift-tube linac (DTL). The beam delivered to the experiment had an energy spread of 0.23% (full width at half maximum, FWHM) and a time spread of 1 ns (FWHM). Because of the presence of rhenium in the ion source, used to provide surface ionization for alkali beams for other experiments in the same schedule, significant quantities of ^{23}Na were present after mass selection as the relative mass difference between ^{23}Na and ^{23}Mg amounts to only $\Delta M/M = 1.896 \times 10^{-4}$. The $A = 23$ beam contained a time-varying intensity of ^{23}Na and an average ^{23}Mg intensity of $2\text{--}3 \times 10^7 \text{ s}^{-1}$ (typical ratios $^{23}\text{Na}:^{23}\text{Mg}$; 20:1 to 1000:1).

A. The DRAGON facility

The beam was guided through the windowless recirculating hydrogen target at DRAGON [17]. Prompt γ rays from proton capture reactions were detected in an efficient 30-element bismuth germanate (BGO) hexagonal detector array surrounding the gas target cell. A single charge state of $A = 24$ reaction recoils and $A = 23$ unreacted beam particles was selected using a set of slits at the first energy-dispersed focus, after the first dipole bending magnet of the separator. The recoils were then selected at a mass-dispersed focus after passing through an electrostatic dipole field. A further stage of filtering used another pair of magnetic and electrostatic dipoles. Recoils were identified using a combination of local time-of-flight measurement with a dual microchannel plate (MCP) system [18], and a ΔE vs. E measurement using an isobutane-filled segmented ionization chamber [19].

The beam energy was measured at the energy-dispersed focus after the first magnetic dipole using a set of 2-mm-wide slits. This magnet has been calibrated using a large set of well-known narrow (p,γ) resonances with stable beams. The precision of such a beam energy measurement was determined to be of the order 0.75A keV in the energy range relevant for this experiment [20]. The stopping power in the gas target was measured by combining beam energy measurements with and without gas in the target.

The position of a resonance in the gas target can be determined by examining a spectrum of the z coordinate of the BGO detectors that received the highest-energy prompt γ rays from the reaction. The centroid of this distribution indicates the position of the resonance within the gas cell. Using this value and the stopping power, it is possible to calculate the beam energy loss up to that position in the gas and therefore determine the resonance energy. This method has been used successfully with other narrow resonance radiative capture reactions at DRAGON [21]. For further discussion of the method of BGO z -coordinate centroid in determining resonance energy, see Secs. IV C and IV D.

TABLE II. Number of ^{23}Mg before and after target entrance aperture and contributions to the uncertainty of the number of Mg ions on target (percentages).

Group	^{23}Mg before aperture	^{23}Mg after aperture	$N_{\text{NaI}}/f_{\text{live}}$ (%)	Transmission (%)	Charge state fraction (%)	NaI efficiency (%)
1	$(2.22 \pm 0.17) \times 10^{12}$	$(2.17 \pm 0.15) \times 10^{12}$	0.8	3.1	4.1	5.5
2	$(1.60 \pm 0.12) \times 10^{12}$	$(1.57 \pm 0.11) \times 10^{12}$	0.7	3.1	4.1	5.5
3	$(5.10 \pm 0.39) \times 10^{12}$	$(4.77 \pm 0.33) \times 10^{12}$	1.1	3.2	4.1	5.5
4	$(2.76 \pm 0.21) \times 10^{12}$	$(2.71 \pm 0.19) \times 10^{12}$	0.2	3.1	4.1	5.5

B. Beam normalization and isobaric contaminants

To determine the number of incident $A = 23$ ions on target as well as the ratio of ^{23}Mg to ^{23}Na , the beam intensity was monitored at several places in the DRAGON separator using a variety of methods. Upstream and downstream of the gas target, the current was measured before and after each run using Faraday cups with a 1σ readout uncertainty of approximately 5 pA. At the mass-dispersed focus after the first electrostatic dipole, mass 23 beam particles of the selected charge state are stopped on one of a pair of slits, whereas the mass 24 recoils are transmitted. The unsuppressed current on these slits was recorded throughout the experiment. The β^+ decay of the ^{23}Mg deposited on the slit was measured via the detection of coincident 511 keV annihilation γ rays using two face-to-face NaI(Tl) detectors located around a “collector horn” which covered a small fraction of the solid angle into which the beam-decay positrons from the slit are emitted [19]. In addition, a scintillator intercepted another portion of the stream of positrons and was used for comparison. An efficiency calibrated high-purity germanium detector (HPGe) was present outside the vacuum enclosure containing the slits in order to monitor the 511 keV and 440 keV γ rays resulting from the β^+ decay of ^{23}Mg on the slits.

The number of ^{23}Mg incident on the H_2 target was calculated using the formula

$$N_{\text{Mg}} = \frac{N_{\text{NaI}}/f_{\text{live}}}{f_{\text{Mg}} \times \epsilon_{\text{target}} \times \epsilon_{\text{NaI}}}, \quad (1)$$

where $N_{\text{NaI}}/f_{\text{live}}$ is the number of detected 511-keV γ -ray coincidences in the NaI detectors, divided by the live-time fraction of the data acquisition system. f_{Mg} is the fraction in the chosen charge state under the current conditions (measured separately using stable beams). ϵ_{target} is the beam transmission into the target region, and ϵ_{NaI} is the efficiency of the NaI detectors for 511-keV coincidences multiplied by the solid angle of the horn. The total number of ^{23}Mg before the target entrance aperture and after the target entrance aperture for the two sets of runs for which $^{23}\text{Mg}(p, \gamma)^{24}\text{Al}$ reactions were seen are given in Table II.

The values and uncertainties of the charge state fractions were taken from our 2007 measurements [10] with uncertainties adjusted by a factor 1.5 to account for the different beam energy (based on predictions of the charge state fraction evolution with energy [18,22]). The 511-keV coincidence efficiencies of the NaI detectors ϵ_{NaI} were calibrated using a beam of radioactive ^{21}Na of known intensity deposited onto the mass slits. Different settings of the electrostatic dipole

in front of the mass slits were investigated to determine the sensitivity of the NaI detectors’ efficiency to small variations in beam position. The magnitudes of these effects were taken into account in the error analysis. The different contributions to the uncertainty can be found listed alongside the number of incident ^{23}Mg in Table II.

C. Particle identification

The particle identification in the experiment was particularly challenging because of the isobaric contamination of the ^{23}Mg beam with ^{23}Na , which via proton capture produce ^{24}Al and ^{24}Mg recoils, respectively.

In order to distinguish valid detections of ^{24}Al recoils from (a) unreacted “leaky” ^{23}Mg beam, (b) unreacted “leaky” ^{23}Na beam, and (c) contaminating ^{24}Mg recoils from the $^{23}\text{Na}(p, \gamma)^{24}\text{Mg}$ reaction, software conditions (or “cuts”) were imposed on the data. These cuts used the recoil singles (detection of heavy ions at the focal plane without reference to whether a prompt γ ray was detected) and, subsequently, γ -ray coincident data. The first-stage means of particle identification came from the ΔE - E information in the ionization chamber (IC). Figure 3 shows incoming mass-23 beam data (taken during a period of unusually low ^{23}Na contamination), where the beam intensity was attenuated to a few hundred per second using a series of fine meshes upstream of the gas target. A particle identification parameter (PID) was defined with the sum of all anode pulse heights (E_{sum}) in the IC and the pulse

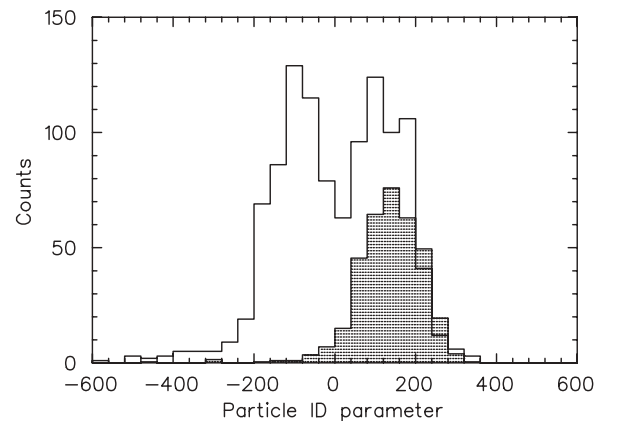


FIG. 3. Particle ID data from ionization chamber for attenuated $A = 23$ beam, showing Mg+Na peaks when lasers are on (unshaded) and Na peak when lasers are off (shaded).

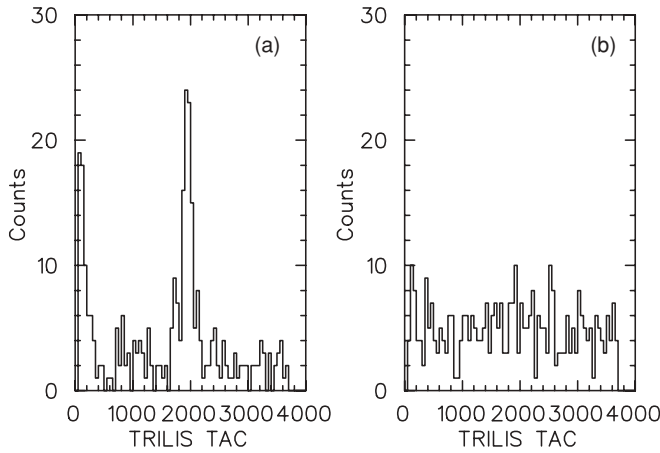


FIG. 4. Time difference between the arrival of detected beam particles at the DRAGON ionization chamber and a laser ion source time signal, for (a) magnesium-like and (b) sodium-like events, under normal laser ionization conditions. Scale is $200 \mu\text{s}$ per 3700 channels.

height in the first anode (ΔE) as $\text{PID} = (E_{\text{sum}} - 3320) - 2(\Delta E - 1440)$. The shaded region shows data taken when the laser ionization was turned off, meaning the magnesium ionization efficiency vanishes while the sodium, primarily from surface ionization, would remain. The unshaded data are those taken when the laser is on, clearly showing a separate magnesium peak at negative particle ID numbers (zero is defined as being the separation point of the two peaks).

Using “clean sodium” ($\text{PID} > 100$) and “clean magnesium” ($\text{PID} < -100$) conditions, gated spectra were produced for timing data, where the detected recoil (or leaky beam) time signal correlated to a timing signal pulsed at 10 kHz provided by the laser ion source. This clearly shows (Fig. 4) that there is a time peak associated with the events identified as “magnesium-like,” with no such peak appearing in the “sodium-like” events, as expected. A similar plot (Fig. 5) when lasers were blocked (but still provided a timing signal) shows the absence of the peak in the “magnesium-like” spectrum.

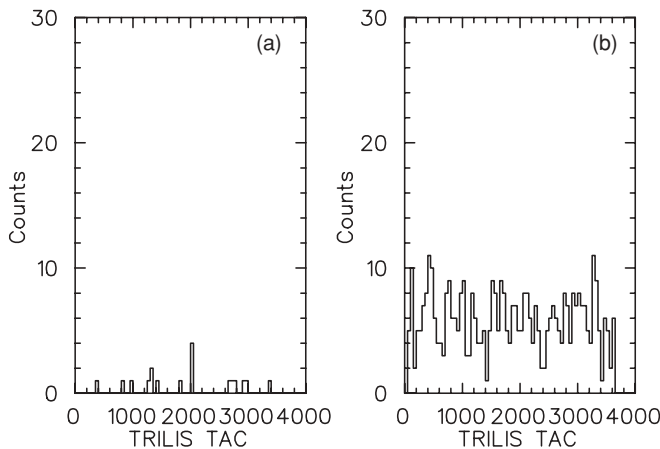


FIG. 5. Time difference between the arrival of detected beam particles at the DRAGON ionization chamber and a laser ion source time signal, for (a) magnesium-like and (b) sodium-like events, when laser ionization is blocked.

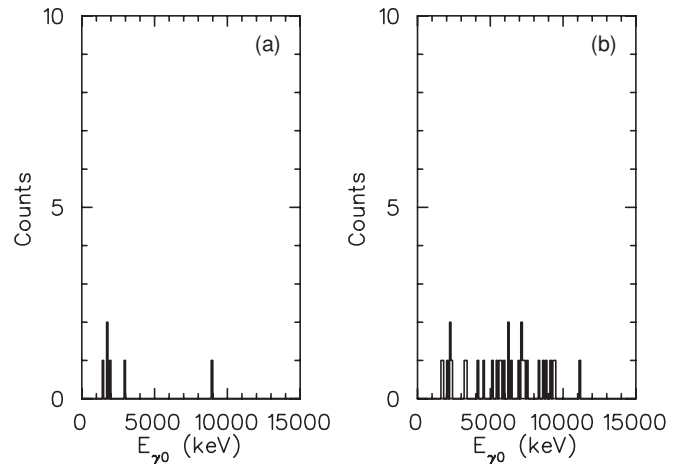


FIG. 6. Highest energy recoil-coincident γ rays ($E_{\gamma 0}$) for (a) “Mg” beam correlated events or for (b) “Na” beam correlated events, separated according to the TRILIS time cuts described in the text.

Placing cuts on the laser-ion-source-correlated timing spectrum around the magnesium peaks and others around the sodium background region, data were taken at full beam intensity and with the separator tuned to accept recoils. Figure 6 shows the energy spectra for the highest-energy recoil-coincident γ rays ($E_{\gamma 0}$) detected. In the spectrum gated on the sodium region, γ -ray energies spanning the region 2.5–12 MeV are seen which cannot come from the $^{23}\text{Mg}(p, \gamma)^{24}\text{Al}$ reaction (which only emits γ rays below 2.4 MeV due to the low Q value). Instead, these events are consistent with the high (11.693 MeV) Q -value reaction $^{23}\text{Na}(p, \gamma)^{24}\text{Mg}$. The magnesium-gated spectrum has only two γ rays above 2.5 MeV, indicating very few “leaky” events through these cuts. These spectra indicate that we are seeing both reactions taking place.

The γ ray energy cuts and other conditions using correlated timing with the accelerator radiofrequency allow us to perform another particle identification calculation where ^{24}Al can be assigned PID values of between -350 and 0 , while positive values indicate ^{24}Mg recoils.

Further illustration of the identification of $A = 24$ ^{23}Mg - and ^{23}Na -induced events can be seen in the following examples. Hereafter, a “singles” event refers to a heavy-ion detection at the focal plane of DRAGON requiring a valid local time-of-flight signal and a valid ionization chamber set of signals. A “coincidence” event refers to the events that satisfy the singles conditions with the addition of having one or more detected γ -ray signals above threshold preceding a heavy ion event within a $9.5\text{-}\mu\text{s}$ time window.

Figures 7, 8, and 9 show recoil data taken from a set of runs at beam energy 502A keV, with a gas target pressure of 3.55 mbar. Figure 7 shows measured local time-of-flight versus total energy detected in the ionization chamber for singles events. The gray density plot indicates “leaky” beam particles, and the empty squares indicate $A = 24$ recoils, showing clear separation of beam and recoil particles. Figure 8 shows the same data in coincidence with a γ ray within the expected coincidence time window. Figure 9 displays an E vs. ΔE

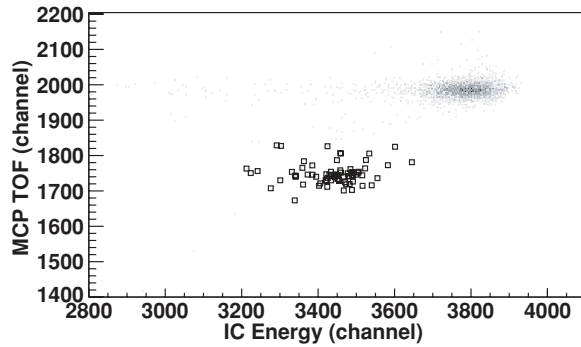


FIG. 7. Local time-of-flight vs. total detected energy for singles recoil events at $E_{\text{beam,lab}} = 502A$ keV and $P_{\text{targ}} = 3.55$ mbar, with the gray density plot indicating all particles detected and the empty squares showing $A = 24$ recoils.

spectrum in the ionization chamber where the $A = 24$ recoils clearly separate into two groups. The empty squares indicate those events satisfying “ $A = 24$ ” mass cuts and the filled circles indicate the subset of events passing the “ ^{24}Al ” PID cuts.

Figure 10 shows coincidence data for these runs with the detected γ energy (Q -value cut) as an additional criterion, illustrating the superior ^{24}Mg background rejection and leaving the ^{24}Al coincidence recoil group. For comparison, data from a pure ^{23}Na beam from the off-line ion source can be seen in Fig. 11 showing the grouping of ^{24}Mg recoils. As mentioned the ^{23}Na content of the mass-23 ion beam varied over nearly two orders of magnitude during this experiment. The selected low ^{23}Na content runs shown here were used to prepare the stringent cuts (applied to the local MCP time-of-flight, the individual five segments of the ionization chamber and the BGO array) for identification of ^{24}Al and ^{24}Mg recoils that were then used in the analysis of the higher ^{23}Na content runs.

The final results of the coincidence identification are presented in Table III. This information is further used in Sec. IV D. Independently, an analysis of the recoil singles relying solely on the MCP time-of-flight and ionization chamber particle identification was performed and our discussion of this is continued in Sec. IV B.

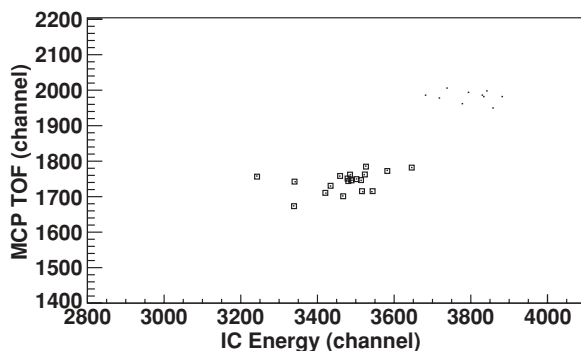


FIG. 8. Local time-of-flight vs. total detected energy for coincidence recoil events at $E_{\text{beam,lab}} = 502A$ keV and $P_{\text{targ}} = 3.55$ mbar, with the black dots indicating all particles detected, and the empty squares showing $A = 24$ recoils.

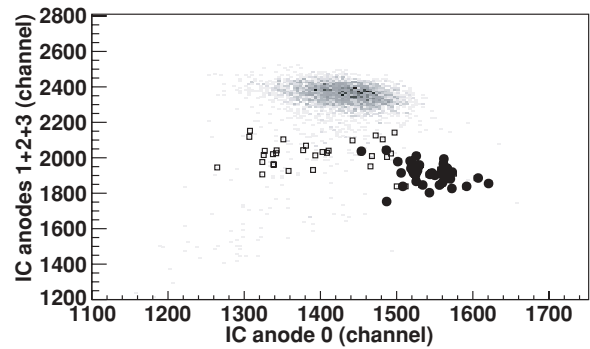


FIG. 9. E vs. ΔE in the ionization chamber for singles events at $E_{\text{beam,lab}} = 502A$ keV and $P_{\text{targ}} = 3.55$ mbar, with the gray density plot indicating all events, the empty squares showing events identified as $A = 24$, and the filled circles being ^{24}Al .

In addition to the number of detected ^{24}Al recoils, the number of detected ^{24}Mg recoils is also extracted from the analysis. Because the $^{23}\text{Na}(p,\gamma)^{24}\text{Mg}$ reaction has a large Q value, and therefore a maximum recoil cone angle that is larger than the acceptance of DRAGON, it is difficult to estimate the normalized yield of the reaction without considerable simulation. Since the $^{23}\text{Na}(p,\gamma)^{24}\text{Mg}$ reaction was not the focus of this experiment, we have not attempted to derive yields but have instead looked at the geometric position of the reaction in the gas target (using the BGO array hit-pattern) in order to determine resonance energies of the $^{23}\text{Na}(p,\gamma)^{24}\text{Mg}$ and $^{23}\text{Mg}(p,\gamma)^{24}\text{Al}$ reactions. Table IV shows the extracted BGO z -coordinate centroids for a selection of runs at different beam energies and target pressures. It can be seen that with the lower target pressure the $^{23}\text{Na}(p,\gamma)^{24}\text{Mg}$ reaction moves to positive (downstream) values. The uncertainties are large because of low statistics, but an estimate of the resonance energy of the $^{23}\text{Na}(p,\gamma)^{24}\text{Mg}$ reaction gives $E_R \approx 475$ keV, which would correspond to an excitation energy of 12.168 MeV (the uncertainty on this value could be as large as 10 keV). No such proton resonance in ^{24}Mg has been reported previously, although the 1990 evaluation of ^{24}Mg energy levels [23] lists a candidate excited state at $E_x = 12.161$ MeV with total width of 0.9 keV observed in the $^{20}\text{Ne}(\alpha,\gamma)^{24}\text{Mg}$ reaction. Our data indicate this resonance has a strength on the order of $100 \mu\text{eV}$, using a rough estimation. A possible explanation for its previous nonobservation by proton capture is that the presence of the strong resonance at 490 keV removed the incentive for carrying out a high-sensitivity experiment at

TABLE III. Summary of coincidence recoil identification among four periods of the experiment.

Group	$E_{\text{beam,lab}}$	P_{targ} (mbar)	Coinc. events	$A = 24$ Recoils	^{24}Al coinc.
1	497A keV	10.39	24	2	0
2	502A keV	9.87	26	11	7
3	502A keV	9.87	1065	54	14
4	502A keV	3.55	29	19	12

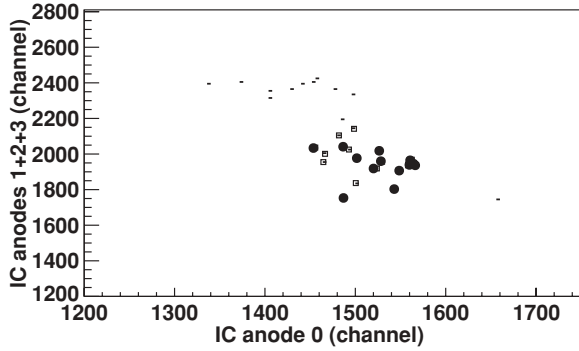


FIG. 10. E vs. ΔE data for coincidence events at at $E_{\text{beam,lab}} = 502\text{A keV}$ and $P_{\text{targ}} = 3.55$ mbar, with the small dots indicating all events, the empty squares showing events identified as $A = 24$, and the filled circles being ^{24}Al .

nearby energies, i.e., there was no strong astrophysical or nuclear structure motivation for making such a measurement.

Extraction of the resonance energy of the $^{23}\text{Mg}(p, \gamma)^{24}\text{Al}$ reaction is more complex, as the events show evidence of being upstream of the center of the gas target. Being limited by low statistics and geometry, the BGO centroid itself is no longer a reliable measure of resonance energy several cm from the center of the target. Therefore Sec. IV D presents an analysis of the full BGO hit pattern of the coincidence $^{23}\text{Mg}(p, \gamma)^{24}\text{Al}$ data as a means to extract a probability distribution for the resonance energy and resonance strength.

IV. ANALYSIS AND INTERPRETATION

This section describes the methods used to extract the strength of the “473 keV” resonance in $^{23}\text{Mg}(p, \gamma)^{24}\text{Al}$. First, it was assumed that the resonance was positioned fully within the gas target, allowing a traditional *thick target yield function* analysis of the data. The value obtained by this method was then compared to the predicted shell-model strength. However, as this difficult experiment was not able to ascertain that the resonance was fully contained in the target, another approach was pursued which determined the energy and strength of the resonance by comparing the coincidence data BGO hit pattern with Monte Carlo simulations.

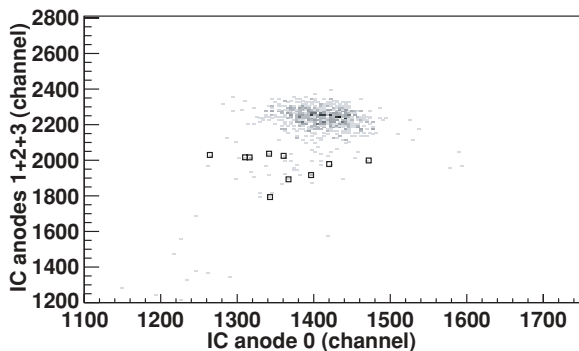


FIG. 11. E vs. ΔE for an off-line ion source run with pure ^{23}Na beam at $E_{\text{beam,lab}} = 502\text{A keV}$, clearly showing position of ^{24}Mg recoils. The gray density plot shows all events with empty squares indicating recoils.

TABLE IV. BGO z -coordinate centroids at different beam energies for $^{23}\text{Mg}(p, \gamma)^{24}\text{Al}$ and $^{23}\text{Na}(p, \gamma)^{24}\text{Mg}$ events. A significant movement of the $^{23}\text{Na}(p, \gamma)^{24}\text{Mg}$ resonance to positive z coordinates when reducing the target pressure is visible.

$E_{\text{beam,lab}}$	Species	P_{targ} (mbar)	$^{23}\text{Mg}(p, \gamma)^{24}\text{Al}$ centroid (cm)	$^{23}\text{Na}(p, \gamma)^{24}\text{Mg}$ centroid (cm)
502A keV	RIB	9.87	-2.8 ± 1.5	-1.4 ± 0.9
502A keV	^{23}Na	9.87	–	-1.5 ± 2.4
502A keV	RIB	3.55	-4.3 ± 1.7	$+3.9 \pm 2.3$

A. Energy loss of ^{23}Mg in gas target

The stopping power of ^{23}Mg was not directly measured during this experiment but instead was inferred from stopping power measurements of ^{24}Mg at the same velocity, since stopping power is isotope-independent to first order. The data for gas target pressure, and corresponding magnetic dipole field strength required to bend ^{24}Mg ions of charge state 8+ to the energy-dispersed focus, are shown in Table V alongside the corresponding calculated values of target thickness and exit ion energy in the laboratory frame.

Using the assumption of a gas temperature of 300 K (measured previously in gas target operation) a stopping power of $\epsilon = 102.8 \pm 5.4$ eV/(10^{15} cm $^{-2}$) was derived. This value agrees well with the $\epsilon = 109.2 \pm 6.5$ eV/(10^{15} cm $^{-2}$) given for Mg at 419A keV in Greife *et al.* [24], but is about 10%–15% lower than the semiempirical estimate calculated with the well-known SRIM code [25].

B. Thick target yield

Using the shell-model value for the resonance strength from the work of Kubono *et al.* ($\omega\gamma = 27$ meV) [7], and the nominal resonance energy of 473 keV, one can calculate the maximum yield, Y_{∞} , from the $^{23}\text{Mg}(p, \gamma)^{24}\text{Al}$ reaction assuming the resonance is fully contained in the target:

$$Y_{\infty} = 2\pi^2 \bar{\kappa}^2 \omega\gamma \frac{M + m}{M} \frac{1}{\epsilon} \quad (2)$$

$$= \omega\gamma \times 2.09 \times 10^{-9} \quad (3)$$

$$= 5.64 \times 10^{-11}. \quad (4)$$

TABLE V. Measuring the beam energy (using charge state 8+) downstream from the gas target for a ^{24}Mg beam with $E = 512.3\text{A keV}$ (12.2875 MeV).

Pressure (mbar)	Magnetic dipole field (tesla)	Target thickness (10^{15} atoms cm $^{-2}$)	Energy (MeV)
0.504 ($\pm 1.5\%$)	(0.3087 \pm 0.0002)	303.4	12.2563
1.063 ($\pm 1.5\%$)	(0.3084 \pm 0.0002)	640.0	12.2325
1.832 ($\pm 1.5\%$)	(0.3078 \pm 0.0002)	1102.6	12.1849
3.095 ($\pm 1.5\%$)	(0.3067 \pm 0.0002)	1863.1	12.0980
5.571 ($\pm 1.5\%$)	(0.3048 \pm 0.0002)	3353.8	11.9486
6.838 ($\pm 1.5\%$)	(0.3038 \pm 0.0002)	4116.7	11.8703

TABLE VI. Summary of $^{23}\text{Mg}(p,\gamma)^{24}\text{Al}$ yield parameters by run group.

Group	Energy (keV/u)	P_{target} (mbar)	Live time fraction	IC events	MCP events	Charge-state fraction
1	497	10.39	0.762 ± 0.00355	1170	1333	0.371 ± 0.050
2	502	9.87	0.775 ± 0.00445	1030	1151	0.371 ± 0.050
3	502	9.87	0.893 ± 0.00227	98640	110044	0.371 ± 0.050
4	502	3.55	0.952 ± 0.00819	3204	3635	0.342 ± 0.050

Here λ is the reduced de Broglie wavelength in the center-of-mass system; M and m are the masses of target and projectile respectively; and ϵ is the laboratory stopping power.

This can be compared to the measured yield, defined as the number of reactions per incoming particle. For this purpose, the detected number of ^{24}Al recoils has to be adjusted by the detection efficiency and transmission of the DRAGON instrument. The appropriate calculation is shown in Eq. (5) and takes into account the number of ^{24}Al detected, ($N_{^{24}\text{Al}}^{\text{det}}$), the measured number of ^{23}Mg delivered on target ($N_{^{23}\text{Mg}}$), the detection efficiency of the microchannel plate (MCP) local time-of-flight system (eff_{MCP}) as well as transmission through the MCP detectors ($\text{trans}_{\text{MCP}}$), the charge state fraction of ^{24}Al at these energies and pressure ($f_{^{24}\text{Al}}$) and the live-time fraction of the experiment (f_{live}). Table VI summarizes these values by run group. The expression for the maximum yield is:

$$Y_{\infty} = \frac{N_{^{24}\text{Al}}^{\text{det}}}{N_{^{23}\text{Mg}} \times \text{eff}_{\text{MCP}} \times \text{trans}_{\text{MCP}} \times f_{^{24}\text{Al}} \times f_{\text{live}}}. \quad (5)$$

Table VII shows the results for the maximum yield using recoil single-particle identification and assuming the thick target yield function applies. The results show a resonance does exist with an apparent strength near that predicted by Kubono [7] and others (but at an energy higher than originally anticipated).

However, while it is clear the resonance does exist, the fact that the resonance was located significantly upstream casts a shadow of doubt on this traditional approach to the analysis. The thick target and BGO array of DRAGON usually permit the experimenter to position the resonance near the center of the gas target. In most cases, this provides certainty that the resonance is fully contained within the target and the thick target equation can be applied. In this case, backgrounds caused by the $^{23}\text{Na}(p,\gamma)^{24}\text{Mg}$ reaction made centering the resonance difficult because higher ^{24}Mg recoil rates would jeopardize the ability to identify ^{24}Al recoils. Therefore an

alternative analysis approach was pursued that will be detailed in the next section.

C. Resonance energy calibration using $^{23}\text{Na}(p,\gamma)^{24}\text{Mg}$

As a check on the energy calibration of the first bending magnet at DRAGON, and the sensitivity of the BGO hit pattern to resonance position in the extended gas target (effective length, $L_{\text{eff}} = 12.3 \pm 0.2$ cm), a beam of ^{23}Na from the off-line ion source with nominal energy 524.8A keV was used. This energy should position the well-known $E_R = 490.4 \pm 0.3$ keV $^{23}\text{Na}(p,\gamma)^{24}\text{Mg}$ resonance in the center of the gas target. Figure 12 shows the resulting recoil- γ coincidence data for the BGO hit-pattern, expressed as a function of the z coordinate of the BGO detector that received the highest-energy γ -ray hit (the origin being the gas cell center). The mean of this distribution indicates the position of the resonance and yields $E_R = 491.3 \pm 1.4$ keV, in good agreement with the accepted value.

D. Determination of resonance strength and energy using γ -ray hit pattern and reaction yield

The coincidence data, after particle identification has been applied, contain two pieces of information. First, the total number of coincidence counts is a measure of the reaction yield, and in the case where the resonance is fully contained in the gas target, the thick-target yield function can be used to extract the resonance strength, $\omega\gamma$. Second, the distribution of coincident γ rays, expressed as a function of the z coordinate of the BGO detector which receives the highest-energy γ ray in any heavy-ion recoil event, is sensitive to the position of the resonance within the extended gas target. This way the γ -ray hit pattern can be used to determine the resonance energy when combined with stopping power information.

To illustrate this point, Fig. 13 shows the distributions of γ rays simulated with GEANT3, for different resonance energies,

TABLE VII. Summary of Y_{∞} for $^{23}\text{Mg}(p,\gamma)^{24}\text{Al}$ by run group ($A = 24$ recoil singles).

Group	Efficiency	Detected ^{24}Al recoil singles	Adjusted recoils	Y_{∞} (reac/ion)
1	0.191 ± 0.027	2	10.5 ± 7.6	$(4.74 \pm 3.43) \times 10^{-12}$
2	0.198 ± 0.028	9	45.5 ± 16.5	$(2.84 \pm 1.05) \times 10^{-11}$
3	0.211 ± 0.031	65	308.8 ± 59.5	$(6.33 \pm 1.24) \times 10^{-11}$
4	0.240 ± 0.033	40	166.6 ± 34.8	$(6.02 \pm 1.28) \times 10^{-11}$

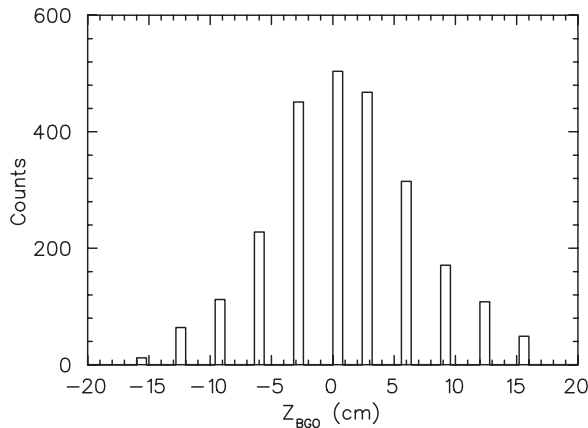


FIG. 12. BGO detector z -coordinate hit pattern of the highest-energy recoil-coincident γ ray in the $^{23}\text{Na}(p, \gamma)^{24}\text{Mg}$ reaction which results in a measured resonance energy of $E_R = 491.3 \pm 1.4$ keV.

one positioned close to the center of the gas target and the other further upstream. In the region between $E_R = 473.5$ keV and 483.5 keV for this reaction, the simulated sensitivity of the BGO z -coordinate mean value is around 0.44 cm/keV. The symmetry of the distribution is also very sensitive to resonance position, and a comparison between data (Fig. 14) and these

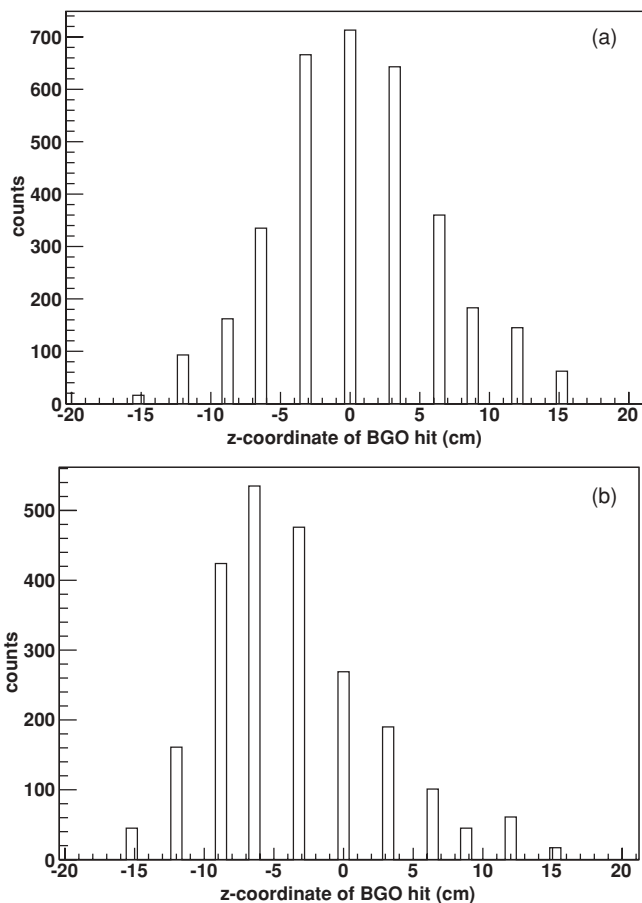


FIG. 13. BGO z -coordinate hit pattern distributions from GEANT3 simulations for $^{23}\text{Mg}(p, \gamma)^{24}\text{Al}$, for fixed beam energy and resonance energies of (a) 473.5 keV and (b) 485.5 keV.

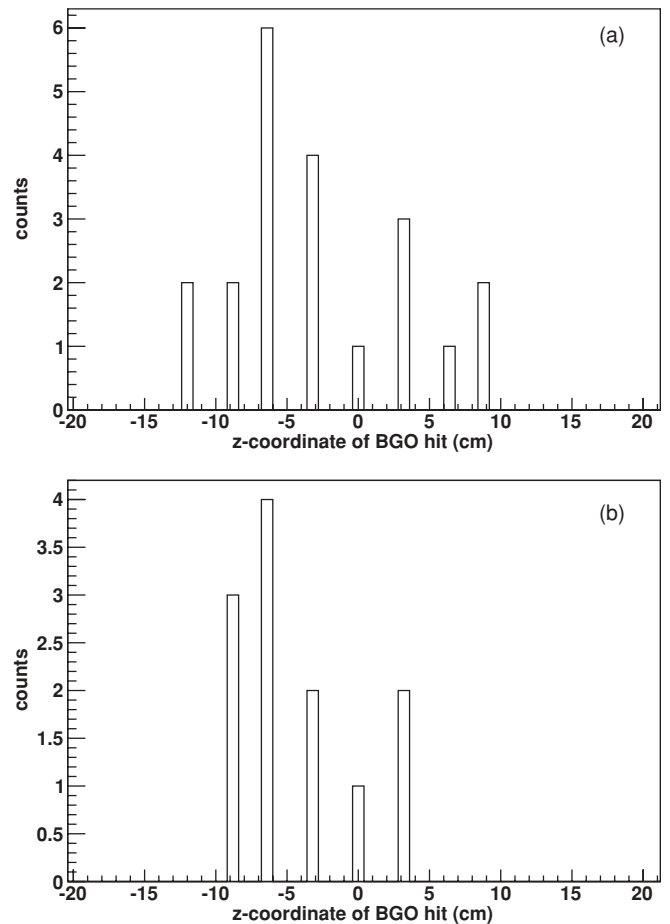


FIG. 14. BGO z coordinate for coincidence events from the $^{23}\text{Mg}(p, \gamma)^{24}\text{Al}$ reaction in runs with beam energy 502A keV and pressures of (a) 9.87 mbar and (b) 3.55 mbar.

simulations is a powerful additional measure of the resonance energy.

Because the coincidence data obtained at a beam energy of 502A keV show distributions which are indicative of an upstream resonance, we cannot be sure that the resonance is entirely in the constant-pressure region of the gas target, and thus the thick target yield function cannot be applied. Instead we use the BGO γ -ray distribution to compare to the expected distributions from GEANT3 simulations and generate a likelihood estimate for each set of coordinates in $(E_R, \omega\gamma)$ space. For a fixed beam energy of 502A keV, a target function is generated that takes into account the measured ISAC beam energy spread, the thermal motion of target atoms, and the energy loss through the gas target, representing the fraction of available target atoms at each incident center-of-mass energy. For every possible value of resonance energy, the reaction yield is generated by integrating the Lorentzian cross section for that energy over the entire target energy range and multiplying by the target function, also including values for the overall BGO efficiency. The Lorentzian is derived from the assumed resonance strength, $\omega\gamma$, and the shell-model partial widths [4]. However, since the resonance width is narrow compared to the

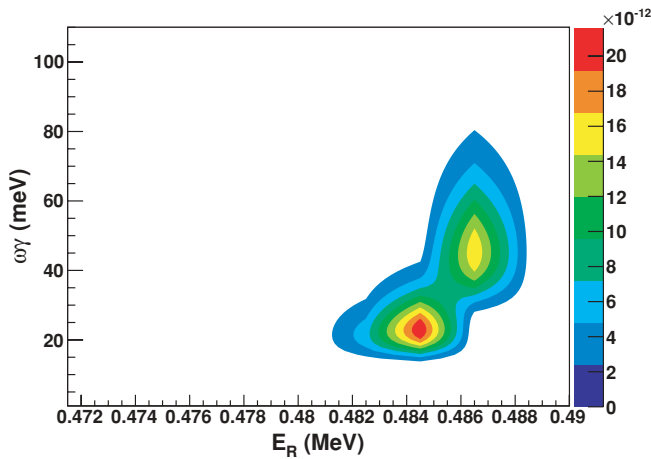


FIG. 15. (Color online) Relative probability contours for resonance strength and resonance energy of first level above proton threshold in $^{23}\text{Mg}(p,\gamma)^{24}\text{Al}$ from comparison of experimental data to GEANT3 simulations (z -scale arbitrary units).

effects of the beam energy spread, etc., it is in reality only the value of $\omega\gamma$ that matters.

A set of GEANT3 simulations with different resonance energies, for both the 3.55-mbar and 9.87-mbar runs, were performed resulting in a distribution of γ -ray hits for each. These predictions are scaled for the number of incident beam particles and the resonance strength, resulting in an array of 11 values for the expected number of counts at each BGO z coordinate, x_i . The real data for each BGO z coordinate are represented by the array n_i . We can then do a comparison between the experimental data and simulated data in terms of the Poisson probability (the probability of observing n_i when x_i is expected):

$$p(n_i; x_i) = \exp(-x_i)(x_i)^{n_i} / n_i! \quad (6)$$

The joint probability for all bins of the BGO z coordinate, $P(n; x) = \prod_i p(n_i; x_i)$, is then constructed. This procedure is performed over a grid of 10 resonance energies and 100 resonance strength values resulting in a two-dimensional probability density function (PDF). The PDFs from the 3.55-mbar and 9.87-mbar runs are combined to give the joint PDF. Also note that the combined error in the number of incident beam ions and the recoil detection efficiency is taken into account at the stage of generating the x_i arrays. Figure 15 shows the resulting two-dimensional probability contours, while Fig. 16 shows the corresponding projections onto the $\omega\gamma$ and E_R axes. We can extract certain moments from the projections of the two-dimensional PDF from Fig. 15 in order to extract best values for $\omega\gamma$ and E_R . Taking the median of each projection, we arrive at central values of $\omega\gamma = 37.8$ meV and $E_R = 485.7$ keV respectively. The 68% confidence intervals for these values are extracted as the 16% and 84% quartiles of the distributions:

$$\begin{aligned} E_R &= 485.7^{+1.3}_{-1.8} \text{ keV} \\ \omega\gamma &= 37.8^{+20.5}_{-15.4} \text{ meV.} \end{aligned} \quad (7)$$

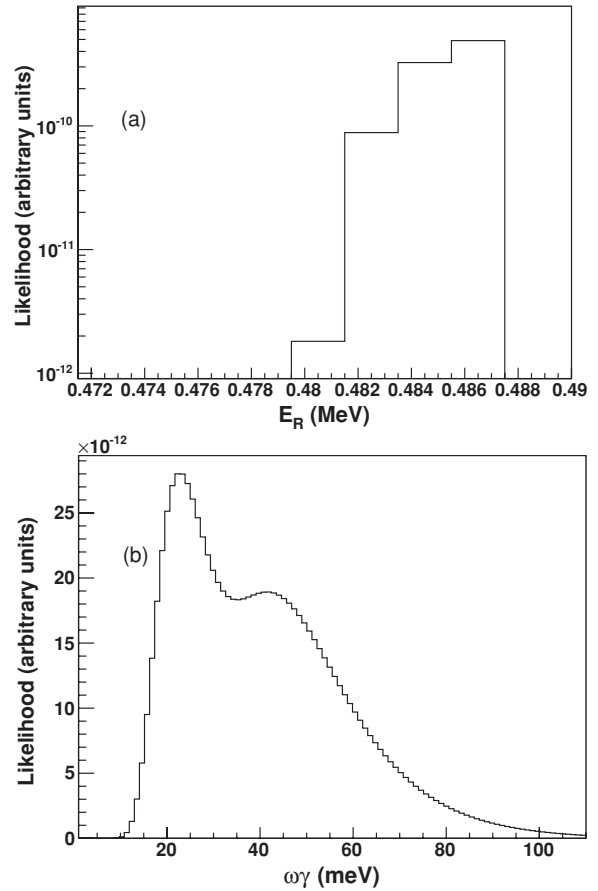


FIG. 16. (a) X and (b) Y projections of the two-dimensional probability distribution in Fig. 15.

The contribution to the total reaction rate from this resonance was generated using a Monte Carlo method. For each temperature, a set of 10,000 random pairs of E_R and $\omega\gamma$ were generated from the two-dimensional PDF of

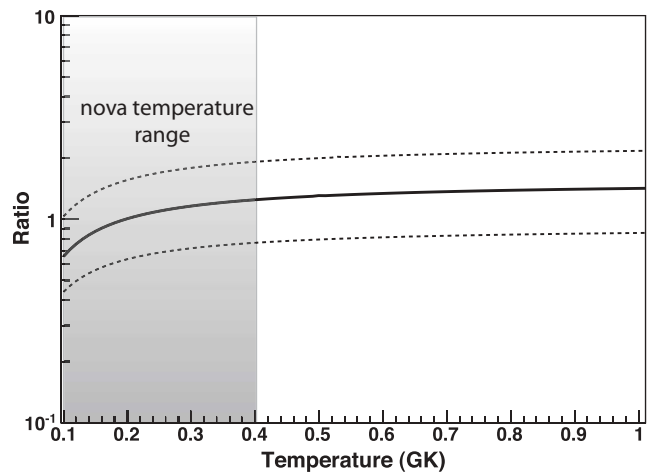


FIG. 17. Ratio of the reaction rate contribution of the “473 keV” $^{23}\text{Mg}(p,\gamma)^{24}\text{Al}$ resonance from this work to the shell-model prediction of Ref. [4]. The 68% confidence limits are shown as dotted lines.

TABLE VIII. Recommended contribution of the first level above proton threshold to the $^{23}\text{Mg}(p, \gamma)^{24}\text{Al}$ rate in units of $\text{s}^{-1} \text{mol}^{-1} \text{cm}^3$, derived from the Monte Carlo rate generation method used on the experimental data. Also listed are the derived 68% and 95% confidence limits.

T_9	Rate ($\text{cm}^3 \text{mol}^{-1} \text{s}^{-1}$)	68% confidence level, lower bound	68% confidence level, upper bound	95% confidence level, lower bound	95% confidence level, upper bound
0.1	6.495×10^{-20}	4.474×10^{-20}	9.259×10^{-20}	3.303×10^{-20}	1.310×10^{-19}
0.11	9.540×10^{-18}	6.522×10^{-18}	1.372×10^{-17}	4.756×10^{-18}	1.928×10^{-17}
0.12	5.864×10^{-16}	3.990×10^{-16}	8.481×10^{-16}	2.889×10^{-16}	1.207×10^{-15}
0.13	1.960×10^{-14}	1.324×10^{-14}	2.852×10^{-14}	9.588×10^{-15}	4.018×10^{-14}
0.14	3.804×10^{-13}	2.573×10^{-13}	5.589×10^{-13}	1.899×10^{-13}	8.006×10^{-13}
0.15	5.133×10^{-12}	3.376×10^{-12}	7.452×10^{-12}	2.432×10^{-12}	1.044×10^{-11}
0.16	4.865×10^{-11}	3.211×10^{-11}	7.105×10^{-11}	2.329×10^{-11}	9.962×10^{-11}
0.17	3.511×10^{-10}	2.284×10^{-10}	5.174×10^{-10}	1.651×10^{-10}	7.265×10^{-10}
0.18	2.030×10^{-9}	1.322×10^{-9}	2.982×10^{-9}	9.750×10^{-10}	4.216×10^{-9}
0.19	9.715×10^{-9}	6.371×10^{-9}	1.438×10^{-8}	4.681×10^{-9}	2.012×10^{-8}
0.2	3.975×10^{-8}	2.563×10^{-8}	5.882×10^{-8}	1.883×10^{-8}	8.373×10^{-8}
0.21	1.410×10^{-7}	9.180×10^{-8}	2.080×10^{-7}	6.610×10^{-8}	2.949×10^{-7}
0.22	4.435×10^{-7}	2.863×10^{-7}	6.548×10^{-7}	2.091×10^{-7}	9.473×10^{-7}
0.23	1.264×10^{-6}	8.109×10^{-7}	1.875×10^{-6}	5.898×10^{-7}	2.707×10^{-6}
0.24	3.276×10^{-6}	2.097×10^{-6}	4.922×10^{-6}	1.532×10^{-6}	6.941×10^{-6}
0.25	7.904×10^{-6}	5.041×10^{-6}	1.183×10^{-5}	3.668×10^{-6}	1.681×10^{-5}
0.26	1.771×10^{-5}	1.127×10^{-5}	2.671×10^{-5}	8.166×10^{-6}	3.770×10^{-5}
0.27	3.744×10^{-5}	2.390×10^{-5}	5.608×10^{-5}	1.719×10^{-5}	7.939×10^{-5}
0.28	7.550×10^{-5}	4.721×10^{-5}	1.125×10^{-4}	3.455×10^{-5}	1.595×10^{-4}
0.29	1.414×10^{-4}	9.041×10^{-5}	2.127×10^{-4}	6.594×10^{-5}	3.006×10^{-4}
0.3	2.588×10^{-4}	1.611×10^{-4}	3.884×10^{-4}	1.175×10^{-4}	5.471×10^{-4}
0.32	7.586×10^{-4}	4.743×10^{-4}	1.145×10^{-3}	3.479×10^{-4}	1.632×10^{-3}
0.34	1.957×10^{-3}	1.228×10^{-3}	2.933×10^{-3}	8.902×10^{-4}	4.131×10^{-3}
0.36	4.510×10^{-3}	2.806×10^{-3}	6.805×10^{-3}	2.070×10^{-3}	9.701×10^{-3}
0.38	9.402×10^{-3}	5.853×10^{-3}	1.426×10^{-2}	4.262×10^{-3}	2.023×10^{-2}
0.4	1.832×10^{-2}	1.130×10^{-2}	2.764×10^{-2}	8.380×10^{-3}	3.957×10^{-2}
0.45	7.366×10^{-2}	4.541×10^{-2}	1.123×10^{-1}	3.328×10^{-2}	1.579×10^{-1}
0.5	2.188×10^{-1}	1.354×10^{-1}	3.353×10^{-1}	9.925×10^{-2}	4.718×10^{-1}
0.55	5.349×10^{-1}	3.270×10^{-1}	8.083×10^{-1}	2.376×10^{-1}	1.158×10^0
0.6	1.091×10^0	6.724×10^{-1}	1.678×10^0	4.902×10^{-1}	2.373×10^0
0.65	2.043×10^0	1.223×10^0	3.087×10^0	8.803×10^{-1}	4.368×10^0
0.7	3.335×10^0	2.045×10^0	5.101×10^0	1.483×10^0	7.286×10^0
0.75	5.066×10^0	3.112×10^0	7.908×10^0	2.268×10^0	1.117×10^1
0.8	7.488×10^0	4.576×10^0	1.147×10^1	3.351×10^0	1.617×10^1
0.85	1.028×10^1	6.205×10^0	1.567×10^1	4.574×10^0	2.212×10^1
0.9	1.372×10^1	8.197×10^0	2.111×10^1	5.980×10^0	2.967×10^1
0.95	1.753×10^1	1.064×10^1	2.662×10^1	7.700×10^0	3.714×10^1
1	2.188×10^1	1.320×10^1	3.347×10^1	9.654×10^0	4.757×10^1
1.25	4.902×10^1	2.907×10^1	7.447×10^1	2.104×10^1	1.059×10^2
1.5	7.782×10^1	4.679×10^1	1.196×10^2	3.358×10^1	1.687×10^2

Fig. 15 and the reaction rate was calculated. From the resulting distribution, at every given temperature, the central value was extracted as the *median* of the distribution, and the upper and lower limits were extracted as the 16% and 84% quartiles, much as for Eq. (7). The resulting set of central values, upper and lower limits, were subsequently fitted with a function of the form $y = (A/T_9^{3/2}) \exp(-B/T_9)$ and a comparison was made with the rate as recommended in the work of Herndl *et al.* [4]. The ratio of our new rate contribution to that of Ref. [4] is shown plotted in Fig. 17 with the 68% confidence limits. Table VIII shows the recommended reaction rate contribution

values for a set of temperatures, along with the 68% and 95% confidence limits.

V. CONCLUSIONS

We have successfully detected ^{24}Al reaction products from the $^{23}\text{Mg}(p, \gamma)^{24}\text{Al}$ reaction using the DRAGON separator, for the dominant “473 keV” resonance at nova temperatures. The resonance energy as measured by DRAGON (deduced using independent stopping power measurements and beam

energies calibrated with well-known stable beam resonances) is higher than the values reported from previous work. This difference can probably be explained by a miscalibrated ^{24}Al mass measurement leading to an erroneous proton separation energy used in the transformation of precision level-energy measurements into resonance energies.

Using a series of Monte Carlo simulations we have determined the central value of the strength of the dominant resonance to be larger than shell-model estimations [4], but consistent within the large uncertainties. Although low statistics and difficulties in addressing beam purity introduced large uncertainties in our measurement, there has been a drastic reduction in the overall uncertainty of the total reaction rate in the nova temperature range. This in turn will lead to a reduction in the uncertainties of ejected ^{26}Al and ^{22}Na in the types of nova model seen in, for example, Ref. [2]. At temperatures lower than those reached in O-Ne classical novae, the rate will still be dominated by direct capture and uncertainties will be related to this component. In addition, for hydrogen-burning scenarios with much higher temperatures, the role of the 651-keV resonance will become more important. At the moment the strength of that resonance remains based on the shell-model estimate.

An independent, high-precision measurement of the energy of the “473 keV” resonance would allow, when combined with the data from this work, a more precise determination of resonance strength and therefore an improved determination

of the reaction rate. This could be done via a precision mass measurement of the ^{24}Al ground state, which when expressed as a Q value for $^{23}\text{Mg}(p,\gamma)^{24}\text{Al}$ and combined with the excitation energy measured via γ -ray spectroscopy in Ref. [5] will give a precise value for E_R . Considering the experimental limitations incurred by the high- ^{23}Na content of the mass-23 ion beam in this experiment, alternatively, another direct measurement with purer ^{23}Mg beam can be made which ensures that the resonance is fully contained in the gas target. However, given the dominant role of this resonance at O-Ne classical novae temperatures, and the global role the $^{23}\text{Mg}(p,\gamma)^{24}\text{Al}$ reaction plays therein, we believe the rate is now determined with sufficient precision to remove this reaction as a significant source of uncertainty in ^{22}Na and ^{26g}Al ejected yields from the classical novae models considered in Ref. [2]. The case for other scenarios (such as AGB stars) where direct capture would dominate remains dependent on theoretical calculations at the present time.

ACKNOWLEDGMENTS

The authors acknowledge the support of the Natural Sciences and Engineering Research Council of Canada (NSERC) in carrying out this work. TRIUMF is federally funded through the National Research Council of Canada (NRC). Also acknowledged is support from the US DOE Office of Science Grant No. DE-FG02-93ER40789.

-
- [1] C. Rowland *et al.*, *Astrophys. J.* **615**, L37 (2004).
 - [2] C. Iliadis *et al.*, *Astrophys. J. Suppl. Ser.* **142**, 105 (2002).
 - [3] D. Visser *et al.*, *Phys. Rev. C* **76**, 065803 (2007).
 - [4] H. Herndl, M. Fantini, C. Iliadis, P. M. Endt, and H. Oberhummer, *Phys. Rev. C* **58**, 1798 (1998).
 - [5] G. Lotay *et al.*, *Phys. Rev. C* **77**, 042802(R) (2008).
 - [6] M. Greenfield *et al.*, *Nucl. Phys. A* **524**, 228 (1991).
 - [7] S. K. S. Kubono and T. Kajino, *Nucl. Phys. A* **588**, 521 (1995).
 - [8] R. Zegers *et al.*, *Phys. Rev. C* **78**, 014314 (2008).
 - [9] G. Audi, A. H. Wapstra, and C. Thibault, *Nucl. Phys. A* **729**, 129 (2003).
 - [10] L. E. Erikson, Ph.D. thesis, Colorado School of Mines, 2008.
 - [11] J. M. Freeman, *Nucl. Instrum. Methods* **134**, 153 (1976).
 - [12] J. C. Overley, P. D. Parker, and D. A. Bromley, *Nucl. Instrum. Methods* **68**, 61 (1969).
 - [13] T. Eronen *et al.*, *Phys. Rev. Lett.* **100**, 132502 (2008).
 - [14] S. D. Hoath *et al.*, *Phys. Lett. B* **51**, 345 (1974).
 - [15] D. R. Goosman *et al.*, *Phys. Rev. C* **4**, 1800 (1971).
 - [16] J. Lassen *et al.*, *AIP Conf. Proc.* **1104**, 9 (2009).
 - [17] D. A. Hutcheon *et al.*, *Nucl. Instrum. Methods A* **498**, 190 (2003).
 - [18] C. Vockenhuber *et al.*, *Nucl. Instrum. Methods A* **603**, 372 (2009).
 - [19] C. Vockenhuber *et al.*, *Nucl. Instrum. Methods B* **266**, 4167 (2008).
 - [20] S. Engel *et al.*, *Nucl. Instrum. Methods A* **553**, 491 (2005).
 - [21] C. Ruiz *et al.*, *Phys. Rev. Lett.* **96**, 252501 (2006).
 - [22] W. Liu, M.Sc. thesis, Simon Fraser University, 2001.
 - [23] P. M. Endt, *Nucl. Phys. A* **521**, 1 (1990).
 - [24] U. Greife *et al.*, *Nucl. Instrum. Methods B* **217**, 1 (2004).
 - [25] <http://www.srim.org>.